Acta Oceanol. Sin., 2021, Vol. 40, No. 11, P. 70–78
https://doi.org/10.1007/s13131-021-1870-7
http://www.aosocean.com
E-mail: ocean2@hyxb.org.cn

Interannual variability in the sea surface cooling induced by tropical cyclones in the South China Sea

Juan Ouyang[1], Chunhua Qiu[1, 2, 3]*, Zhenhui Yi[1], Dongxiao Wang[1, 2, 3, 4], Danyi Su[5], Hong Liang[1], Zihao Yang[1]

[1] School of Marine Sciences, Sun Yat-sen University, Guangzhou 510275, China

[2] Southern Marine Science and Engineering Guangdong Laboratory (Zhuhai), Zhuhai 519020, China

[3] Pearl River Estuary Marine Ecosystem Research Station, Ministry of Education, Zhuhai 519020, China

[4] Guangdong Provincial Key Laboratory of Marine Resources and Coastal Engineering, Zhuhai 519020, China

[5] Hydrate Engineering Technology Center, China Geological Survey, Guangzhou 510760, China

Received 15 April 2021; accepted 21 June 2021

Abstract

Sea surface cooling induced by tropical cyclones (TCs) is an important component of air-sea interactions. Using coordinate transformation and composite analysis methods, we examined the interannual variability in TC-induced sea surface cooling (TCSSC) in the South China Sea (SCS). The frequency of surface cooling cases was over 86% and that of surface warming cases was less than 14%. The magnitude of TCSSC was defined as the absolute value of TCSSC. The maximum magnitude of TCSSC occurred on the right side of the TC track, and the mean magnitude of TCSSC decreased by 0.04°C/a from 2006 to 2018. The interannual variability in TCSSC was highly correlated with the TC translation speed and pre-TC mixed layer depth. Notably, TCSSC got enhanced in El Niño years of 2007, 2010, and 2015. The El Niño types were suggested to determine the occurring periods of strong TCSSC via controlling the positions of SCS anticyclones, which brought pre-TC shallow mixed layer and caused strong TCSSC via vertical mixing process during El Niño events. To quantify how the anticyclone influences TCSSC, we need to use mixed layer heat balances model in the next study.

Key words: sea surface cooling, tropical cyclone, El Niño-Southern Oscillation (ENSO), South China Sea, anticyclone

Citation: Ouyang Juan, Qiu Chunhua, Yi Zhenhui, Wang Dongxiao, Su Danyi, Liang Hong, Yang Zihao. 2021. Interannual variability in the sea surface cooling induced by tropical cyclones in the South China Sea. Acta Oceanologica Sinica, 40(11): 70–78, doi: 10.1007/s13131-021-1870-7

1 Introduction

Tropical cyclones (TCs) occur frequently in the western North Pacific (WNP) (D'Asaro et al., 2011), and are one of the most destructive natural disasters, causing tremendous economic damages and loss of lives. TCs can trigger strong surface cooling by enhancing air-sea heat fluxes and oceanic vertical mixing, with the former accounting for 15% of sea surface cooling and the latter for 85% (Price, 1981). The TC-induced sea surface cooling (TCSSC), in turn, can reduce TC's intensity, because TCs tend to weaken (strengthen) when passing cold (warm) water (Brand, 1971; Cione and Uhlhorn, 2003; Lin et al., 2005). In a coupled model, the negative sea surface temperature (SST) feedback produced by a TC could reduce the TC intensity by more than 50% (Schade and Emanuel, 1999). In addition, TCSSC can affect local atmospheric conditions (Lin et al., 2003b) as well as global climate changes (Sriver and Huber, 2010). Therefore, the study of TCSSC is of great significance.

TCSSC usually ranges in 0–5°C (Leipper, 1967; Cione and Uhlhorn, 2003; D'Asaro et al., 2007; Wang et al., 2016) and mostly exhibits a rightward bias in the Northern Hemisphere (Leipper, 1967; Price, 1981; Shay et al., 1992; Price et al., 1994), although a few researchers have argued that maximal TCSSC is not only found on the right side but also on the left side of the TC track (Leipper, 1967; Ko et al., 2014). TCSSC has a recovery time of 7 d to 1 month (Hazelworth, 1968; Price et al., 2008; Dare and McBride, 2011).

Statistical analyses show that TCSSC might be related to TCs' properties (i.e., intensity, translation speed, and size) and the pre-TC oceanic states. Generally, the more intense and slower the TC is, the larger magnitude the TCSSC reaches (Mei and Pasquero, 2013). Pre-TC oceanic conditions can also impact the magnitude of TCSSC. For example, a warm eddy can suppress the vertical mixing process, thus weakening TCSSC. Lin (2012) found that the most intense tropical cyclone of 2003 Maemi could not induce obvious TCSSC due to pre-storm warm eddies. Wang et al. (2016) used Argo profiles to construct the three-dimensional structure of upper-layer responses to TCs over the WNP, which suggested that the deeper (shallower) the mixed layer extended, the weaker (stronger) the TCSSC was. Mei et al. (2015) compared TCSSC in the South China Sea (SCS) and the WNP and found that the mixed layer is shallower in the SCS than in the WNP, resulting in larger magnitude of TCSSC in the SCS.

The SCS is the largest marginal sea of the WNP and has a high concentration of TCs (10.3 per year), some of which form in the

Foundation item: The National Natural Science Foundation of China under contract No. 41976002.
*Corresponding author, E-mail: qiuchh3@mail.sysu.edu.cn

WNP (7.8 per year) and the others generate locally in the SCS (Wang et al., 2007). There are several case studies of TCSSC in the SCS. Using the Princeton Ocean Model, Chu et al. (2000) demonstrated that TCSSC occurrences in the SCS were similar to those in the open ocean. Lin et al. (2003a) revealed that the magnitude of TCSSC in the SCS can reach 10°C. An extreme cooling caused by TC Kai-Tak was identified by Chiang et al. (2011), which was due to slow translation speed of TC and anomalous pre-storm oceanic states (abnormal warm SST and shallow mixed layer). Ko et al. (2014) identified another profound TCSSC of 8°C in the SCS, and the cold wake occurred on both sides of the TC track. This intense TCSSC was suggested to be influenced by the shallow pre-storm thermocline, the slow translation speed of the TC, the distinctive geographical setting, and monsoons. Based on these findings, it is understood that the magnitude of TCSSC varies greatly among different cases. Thus, it is necessary to explore the statistical characteristics of TCSSC and examine the possible mechanisms in the SCS.

With increasing amounts of observational data, numerous studies have investigated the interannual variability in TCs in the SCS. Chan (2000) reported that more TCs occur in the SCS in the autumn before an El Niño year, while fewer TCs occur in El Niño years. Goh and Chan (2010) reported that fewer (more) TCs pass the SCS during El Niño (La Niña) years compared to normal years. Chang et al. (2020) found that TC translation speeds have increased in the SCS (+0.077 m/s per year), regardless of interannual variability, in the past 20 years. Most studies demonstrated that the El Niño-Southern Oscillation (ENSO) is the key factor influencing TC activity in the SCS. However, the spatiotemporal variability and mechanisms of TCSSC as well as how the ENSO influences the amplitude of TCSSC have seldom been studied in the SCS.

In the present study, we investigated interannual variability in TCSSC during the period of 2006–2018 in the SCS, and examined the underlying mechanisms. Data and methods were presented in Section 2, spatiotemporal characteristics of SST changes were discussed in Section 3, possible mechanisms were discussed in Section 4, and conclusions were presented in Section 5.

2 Data and methods

2.1 *Data*

TC data including 6-hourly positions, intensities, central pressures, 2-min average sustained wind speeds, and the longest radius of 30-kn (~15 m/s, 1 kn = 0.514 444 4 m/s) wind speeds (R_{30}) from 2006 to 2018 were used. The former four parameters were derived from the China Meteorological Administration (http://tcdata.typhoon.org.cn/zjljsjj_zlhq.html) (Ying et al., 2014), while the R_{30} data were obtained from the Japan Meteorological Agency best track dataset (http://www.jma.go.jp/jma/jma-eng/jma-center/rsmc-hp-pub-eg/trackarchives.html). We calculated the translation speed at each TC centre using the central difference method. On average, 12.4 TCs passed through the SCS annually. All 161 TC tracks in the SCS from 2006 to 2018 were shown in Fig. 1.

Daily SST data were obtained from the Operational SST and Sea Ice Analysis (http://data.nodc.noaa.gov/ghrsst/L4/GLOB/UKMO/OSTIA). The data were designed for high spatial and temporal resolution applications including marine applications, global numerical weather prediction, and global climate monitoring. Using a multi-scale optimal interpolation method, this set of SST data combined satellite and *in situ* observations and had a bias of 0.17 K and a root mean square error of 0.39 K (Stark et al., 2007). We used the daily 0.05° gridded SST data from 2006 to 2018 to examine TCSSC.

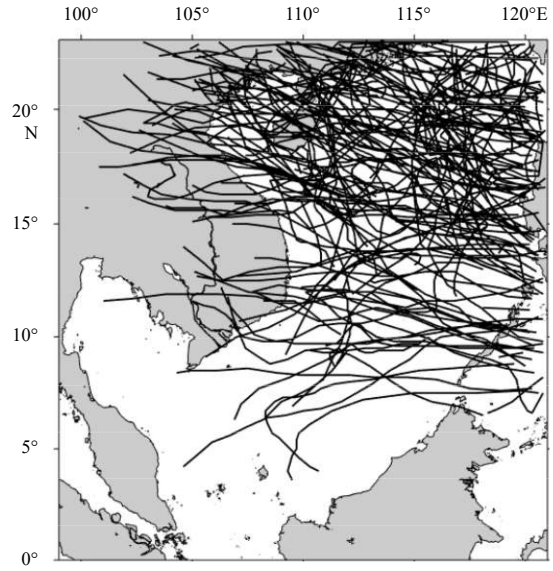

Fig. 1. Tracks of TCs in the SCS from 2006 to 2018.

The WindSat daily surface wind data with a horizontal resolution of 0.25° × 0.25° were download from the remote sensing systems website (http://data.remss.com/windsat/). The WindSat multi-frequency polarimetric microwave radiometer was developed by the Naval Research Laboratory for the U.S. Navy and the National Polar-orbiting Operational Environmental Satellite System Integrated Program Office. The polarimetric microwave radiometer can measure ocean surface wind vectors. The data have been calibrated and validated and are available from February 2003 to the present.

The sea water temperature data were collected by the International Argo Program and the national programs (Argo, 2021; https://argo.ucsd.edu). The mixed layer depth (MLD) was defined as the depth where the vertical temperature gradient had maximum absolute value.

2.2 *Methods*

2.2.1 *Coordinate transformation method*

Because most TCs in the SCS belong to low intensity (below category 2) TCs, we used the R_{30} as the radius of maximum wind speed (Fig. 2). Approximately 93% of TCs had an $R_{30} \leqslant 500$ km (Fig. 2b). Therefore, we set the box size to 500 km × 500 km to study TCSSC. We also examined the box size of 200 km× 200 km and found that spatial distributions of TCSSC was insensitive to the box size. In total, 2 194 boxes were captured and used to analyse the temporal and spatial variability in TCSSC.

Using the TC centre as the original point, the box was divided to four quadrants as TC response areas. The red square in Fig. 3 indicates the response area. The TCSSC was calculated as follows: $\Delta\mathrm{SST} = \overline{\mathrm{SST}}_{\mathrm{post}} - \overline{\mathrm{SST}}_{\mathrm{pre}}$, where $\overline{\mathrm{SST}}_{\mathrm{pre}}$ and $\overline{\mathrm{SST}}_{\mathrm{post}}$ were the weekly averaged SST before and after the TC passes, respectively. The magnitude of TCSSC was defined as the absolute value of TCSSC. The cooling usually lasted for 1 week (Jansen et al., 2010; Dare and McBride, 2011), thus we used a temporal window size of 7 d.

By rotating the coordinates, we obtained the transferred coordinates of TCSSC in the red box (Fig. 3b). We set the real TC

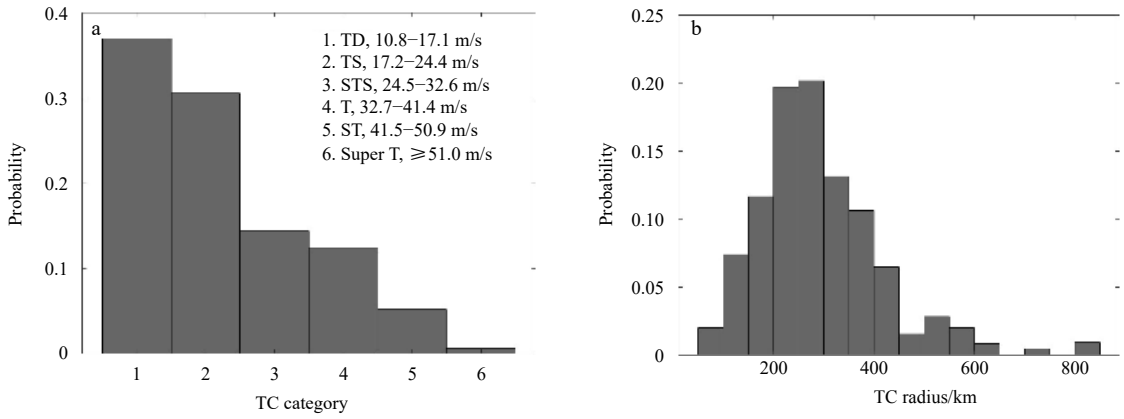

Fig. 2. Probabilities of tropical cyclone (TC) category (a) and radius (b) in the SCS. 1–6 in a reprecent the tropical depression (TD), tropical storm (TS), super tropical storm (STS), typhoon (T), strong typhoon (ST), and super typhoon (Super T), respectively, classified by wind speed . The TC radius in b is defined as the longest radius of 30-kn (~15 m/s) wind speeds.

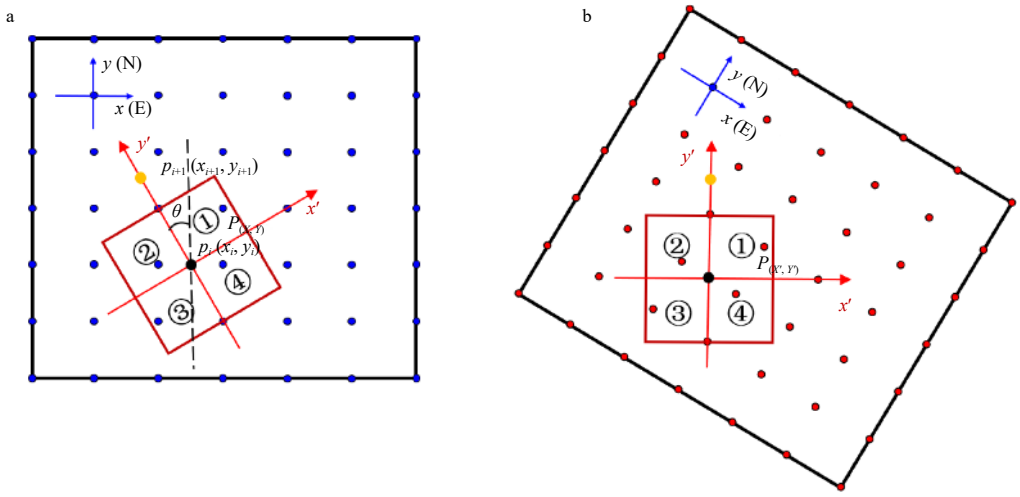

Fig. 3. Schematic diagram of the rotating coordinate system of original (a) and transferred (b) coordinate systems. The red box is the SST response zone. x and y direct eastward and northward, respectively, y' points to the direction of TC translated, and x' is perpendicular to y'. The black dot indicate point p_i at time i, and the yellow dot indicate the next position p_{i+1} at time i+1.①,②,③ and ④ represent the first, second, third and forth quadrant, which take the direction of TC as the positive y'-axis.

track as the y'-axis, whose positive direction was from the original point p_i at time i (black dot) to the next TC centre position p_{i+1} at time i+1 (yellow dot). The x'-axis was perpendicular to y' and directed rightward. Then we obtained the new position of the TCSSC distribution area $P_{(X_i', Y_i')}$ using the following coordinate conversion formula:

$$\begin{cases} X_i' = -x_i + X_i\cos\theta + Y_i\sin\theta, \\ Y_i' = -y_i - X_i\sin\theta + Y_i\cos\theta, \end{cases} \tag{1}$$

where $P_{(X_i, Y_i)}$ was the original coordinates of TCSSC in the red box, and (x_i, y_i) was the position of the TC centre.

As shown in Fig. 3b, the first and fourth quadrants corresponded to the right side of the TC track, while the second and third quadrants were on the left side of the TC track.

2.2.2 *Wind stress curl*

The wind stress curl was calculated as follows:

$$\text{curl}\,(\tau) = \frac{\partial \tau_x}{\partial y} - \frac{\partial \tau_y}{\partial x}, \tag{2}$$

where $\tau_x = \rho_a C_D |U_{10}| u$ and $\tau_y = \rho_a C_D |U_{10}| v$ were the wind stress along the x- and y-directions. ρ_a was the mean air density (1.25 kg/m^3), $|U_{10}|$ was the wind speed magnitude at 10 m height, and u and v were the wind speed magnitude along the x- and y-directions at 10 m height, respectively. The drag coefficient C_D was expressed as (Large and Pond, 1981):

$$C_D = \begin{cases} 1.2 \times 10^{-3}, & |U_{10}| < 11\ \text{m/s}, \\ (0.49 + 0.65 \times |U_{10}|) \times 10^{-3}, & 11\ \text{m/s} \leqslant |U_{10}| < 25\ \text{m/s}, \\ 2.115 \times 10^{-3}, & |U_{10}| \geqslant 25\ \text{m/s}. \end{cases} \tag{3}$$

3 Spatiotemporal characteristics of TCSSC

3.1 *Spatial distribution of TCSSC*

We examined the spatial variability of ΔSST in the 2 194 boxes

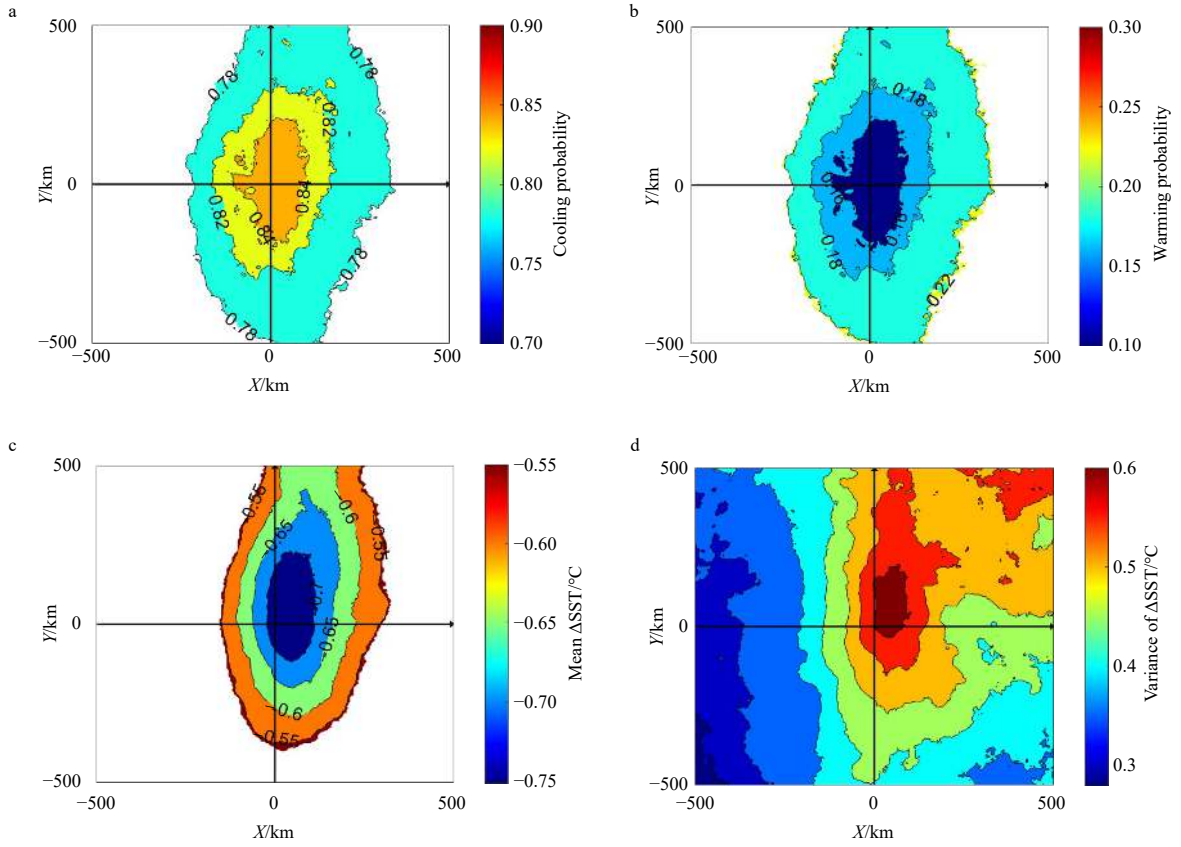

Fig. 4. Probability of TC-induced surface cooling (a) and warming (b), and mean ΔSST (c) and variance of ΔSST (d).

one by one. The probabilities of TCSSC (ΔSST<0°C) and warming (ΔSST>0°C) were shown in Fig. 4. They exhibited elliptical patterns and the maximum probability (~86%) located on the right side of the TC track (Fig. 4a). The probability of ΔSST⩽ –0.70°C was greater than 84% around the TC centre, the area of which covered ~50 000 km^2.

The mean and variance of ΔSST were presented in Figs 4c and d. The centre of TCSSC also had a right-biased ellipse shape, which was consistent with previous reports (Wang et al., 2016). The average magnitude of TCSSC in the SCS was comparable to that in the WNP (~1°C) (Mei and Pasquero, 2013). When only taking TCs with 50-kn maximum sustained winds into account, the mean TCSSC value was –1.4°C in the WNP (Wang et al., 2016). The variance of TCSSC was more than 0.5°C, particularly in the first quadrant. This indicates that the magnitude of TCSSC varied widely on the right front side of TC track.

3.2 *Interannual variability in TCSSC*

Figure 5 depicted maps of the mean ΔSST of all TCs in each year from 2006 to 2018. The amplitudes of regional mean TCSSC in years of 2007, 2010 and 2015 were greater than 1°C, while it was smaller in other years. The cooling areas (ΔSST<–0.7°C) were also larger in above three years than those in other years.

Interannual variability in mean absolute value of TCSSC |ΔSST| was shown in Fig. 6a. The absolute magnitude of TCSSC decreased at a rate of 0.04°C/a from 2006 to 2018, and the TC number increased at a rate of 0.23 a^{-1}, with statistical significance (above the 95% confidence level). This is inconsistent with that in the WNP, where the number of TCs decreased from 1998 to 2015 (Chang et al., 2020). The mean translation speed of TCs also increased gradually. This was consistent with the report of Chang et al. (2020), who found that TC translation speeds increased over the SCS in the last two decades. The mean central pressure had a slightly increase, and the mean TC radius decreased from 2006 to 2018. The relationship between TC properties and TCSSC was presented in the following section.

4 Possible mechanisms of interannual variability in TCSSC

According to previous studies, the magnitude of TCSSC may be related to the TC properties and the pre-TC oceanic states. Here, we discussed their effects on the TCSSC in the SCS.

4.1 *Effects of TC properties*

We examined the relationship between the absolute value of TCSSC |ΔSST| and TC properties, in terms of TC's radius, number, intensity (central pressure) and translation speed (Figs 6b and c). The |ΔSST| and the translation speed/TC number had a negative correlation with a correlation coefficient of –0.83 and –0.45, respectively; however, the correlation between |ΔSST| and TC intensity (central pressure)/radius was not significant. To elucidate the relationship between |ΔSST| and TC intensity, we plotted the mean |ΔSST| and mean TC pressure every 5 hPa in Fig. 7a. The maximum |ΔSST| occurred when the central pressure was below 950 hPa, after which the correlation between |ΔSST| and central pressure was not significant. The magnitude of TCSSC ranged from 1.5°C to 1.9°C when the central pressure was greater than 950 hPa. In addition, stronger TCs induced larger standard deviations of |ΔSST|, indicating that the TC intensity influenced the variability in amplitude of TCSSC. The magnitude of TCSSC was generally negatively correlated with the TC translation speed

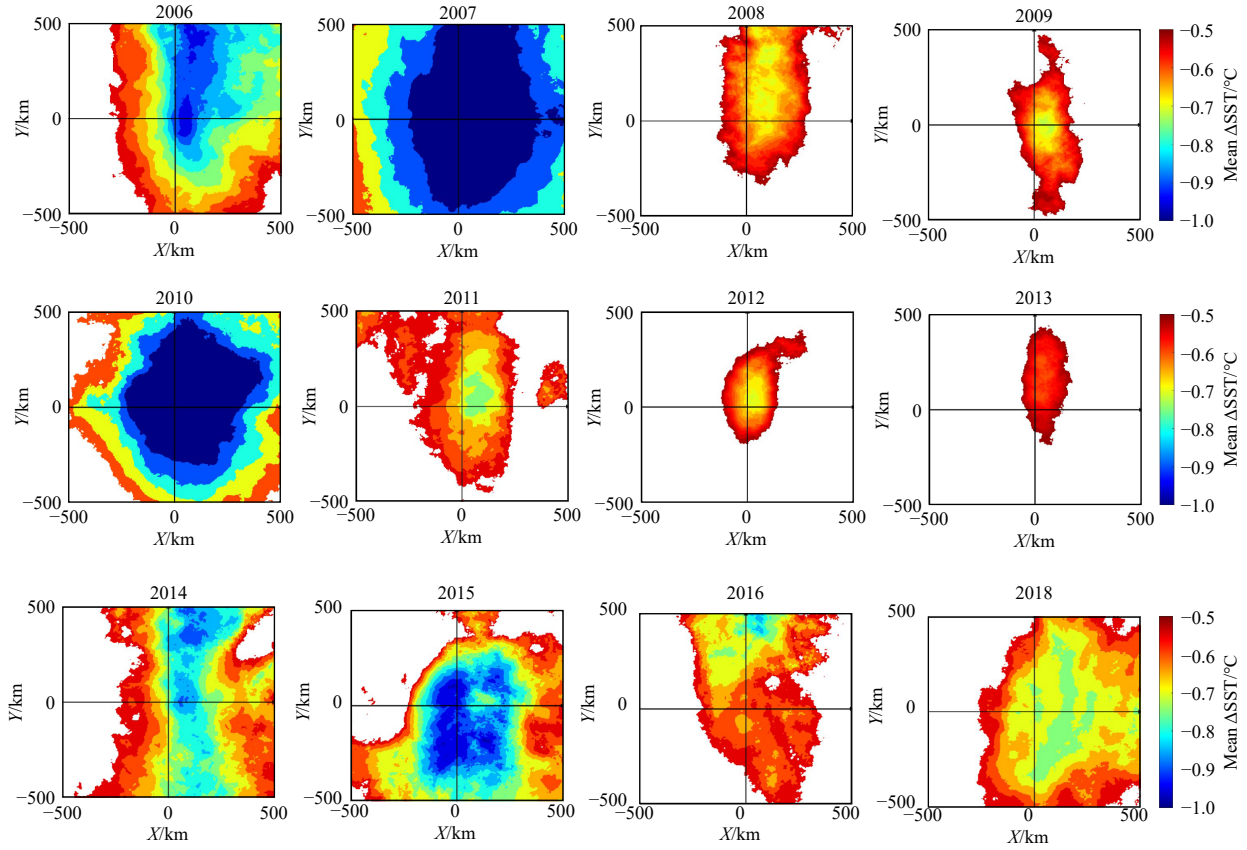

Fig. 5. Spatial distributions of mean TC-included sea surface cooling ΔSST from 2006 to 2018.

at a rate of –0.06°C per 1 m/s (Fig. 7b). The magnitude of TCSSC exceeded 1.2°C when the translation speed was less than 5 m/s.

4.2 *Effect of pre-TC oceanic state*

The upper mixed layer played important roles in regulating TCSSC (Mei et al., 2015; Chang et al., 2020). Here, we examined their effects on the interannual variability in TCSSC in the SCS. Figure 6d showed the interannual variability in averaged MLD and SST around the TC center within 7 d before TC. Here, the mean MLD was calculated as:

$$\overline{H}_{\mathrm{MLD}} = \left(\sum_{i=1}^{I} \sum_{j=1}^{J} \sum_{n=1}^{N} H_{i,j,n} \right) / (I \cdot J \cdot N) , \tag{4}$$

where I=16 and J=16 were the selected grid number around TC center, N was the number of TC position as mentioned in Section 2.2.1, and H was the mean MLD within seven days before TC.

The correlation coefficient between MLD and |ΔSST| was –0.35. The three lowest values of MLD appeared in 2007, 2010, and 2015, while the absolute values of TCSSC were also largest in these three years. This negative correlation was consistent with former studies that a pre-storm shallow mixed layer induced the increased TCSSC (Price, 1981; Lin, 2012; Wang et al., 2016; Chang et al., 2020). We also examined the interannual variability in pre-TC SST, which was positively correlated with TCSSC. The shallow pre-TC MLD and high SST were helpful in enhancing TCSSC.

4.3 *Effect of ENSO*

High TCSSC occurred during El Niño events (Fig. 6c). We attempted to examine whether TCSSC was regulated by the El Niño events. We utilized composite analyses of ΔSST, wind speed, and wind stress curl under El Niño (Niño3.4 index>1), La Niña (Niño3.4 index<–1), and normal conditions (–1 ⩽ Niño3.4 index ⩽ 1). Since the TCSSC had a 6-month lag than Niño3.4 index (Fig. 6a), we matched up the ΔSST on TC time with Niño3.4 index 6 months before TC. Composite TCSSC and wind stress curl distributions were shown in Fig. 8. The absolute magnitude of mean TCSSC was largest during El Niño years and smallest during normal years (Figs 8a–c).

Price (1981) suggested that TCSSC was dominated by vertical pumping. The Ekman pumping velocity was, $w_e = \mathrm{curl}(\tau)/\rho f$, where ρ and f were the water density and Coriolis parameter, respectively. The wind stress curl was maximal during El Niño years and minimal during normal years (Figs 8d–f), indicating that TCSSC was also influenced by Ekman pumping in our study area.

Note that TCSSC was significant in El Niño years of 2007, 2010 and 2015, but was not strong in El Niño year of 2016. To examine this difference, we calculated the wind speed anomaly in above four years. Anticyclones were located over the northern SCS in summer to autumn of 2007, 2010 and 2015, but there was no anticyclone over the SCS in 2016 (Fig. 9). Years of 2007 and 2010 were strong Central Pacific (CP) El Niño events, while 2015 and 2016 were Eastern Pacific (EP) El Niño events (Zhao and Wang, 2019). During CP El Niño events, anticyclones formed in autumn and persisted until the following summer (Wang et al., 2008, 2018), and anticyclones were located over the SCS during the developing stage of an EP El Niño (Yuan et al., 2012). That was consistent with our result that an anticyclone was over SCS in 2015, which

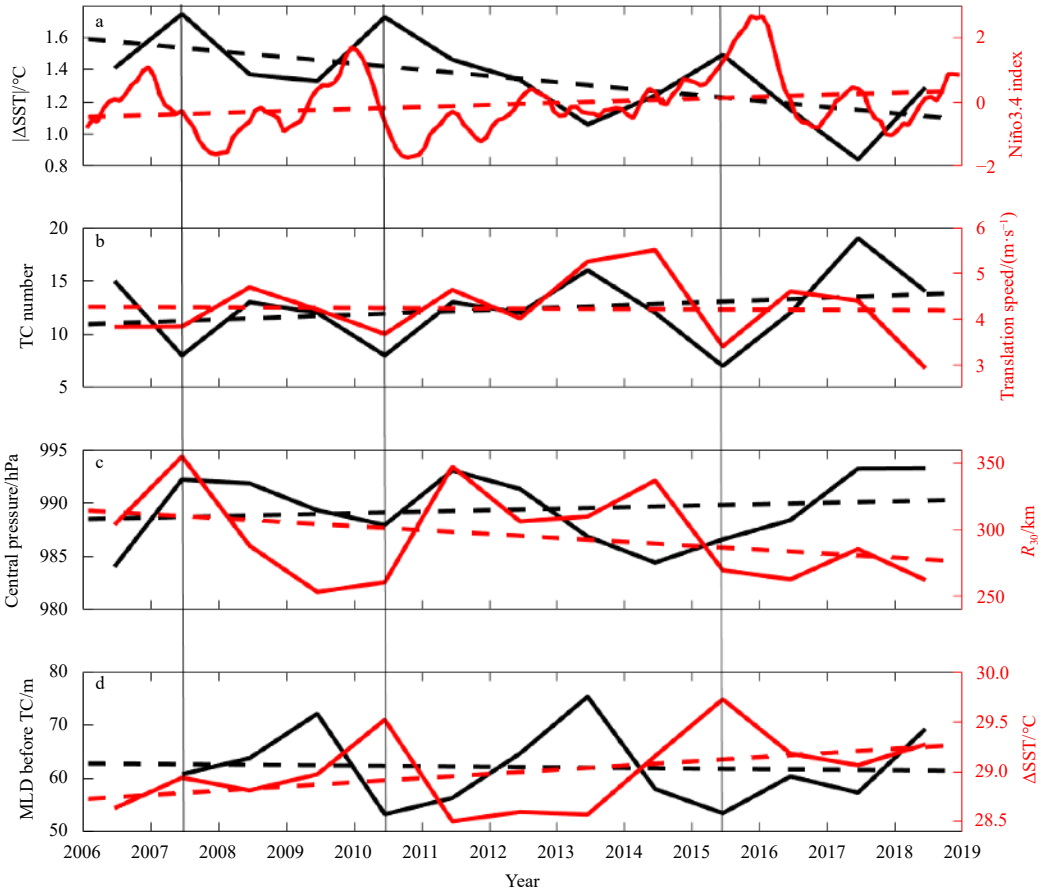

Fig. 6. Interannual variability of TC-included sea surface cooling |ΔSST| (black) and the Niño 3.4 index (red) (a); the number (black) and translation speed (red) of TCs (b); the mean central pressure (black) and radius (red) of TCs (c); and the pre-TC mixed layer depth (MLD) and pre-TC SST around the TC center (d). The dashed lines are linear regression lines.

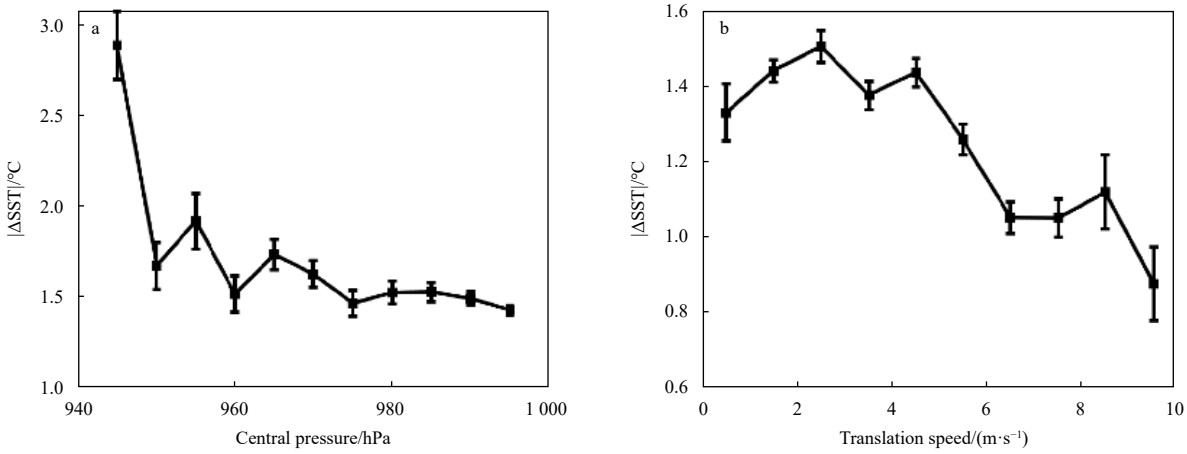

Fig. 7. Relationships between the absolute value of TC-included sea surface cooling (ΔSST) and TC central pressure (a), and TC translation speed (b). Error bars indicate the standard deviation of |ΔSST| at every 5 hPa (a) and every 1 m/s (b).

was at the developing stage of EP El Niño events, rather than 2016.

Low-level anomalous anticyclone has positive effects for SST increase. It usually causes downward motions and reduce precipitation and cloud, causing the increase of the downward shortwave radiation and the decrease of the air-sea latent heat fluxes, and is expected to induce the increase of SST. The high SST may enhance the upper layer stratification and trigger shallow mixed layer. Then the pre-TC ocean states with high SST and shallow mixed layer were easily stirred up by TCs, and finally resulted in strong TCSSC. Wu et al. (2014) suggested ENSO induced high SST due to latent heat fluxes in August and east winter monsoon induced high SST due to short wave radiation in the SCS. To quantify how the anticyclone influences pre-TC SST and MLD,

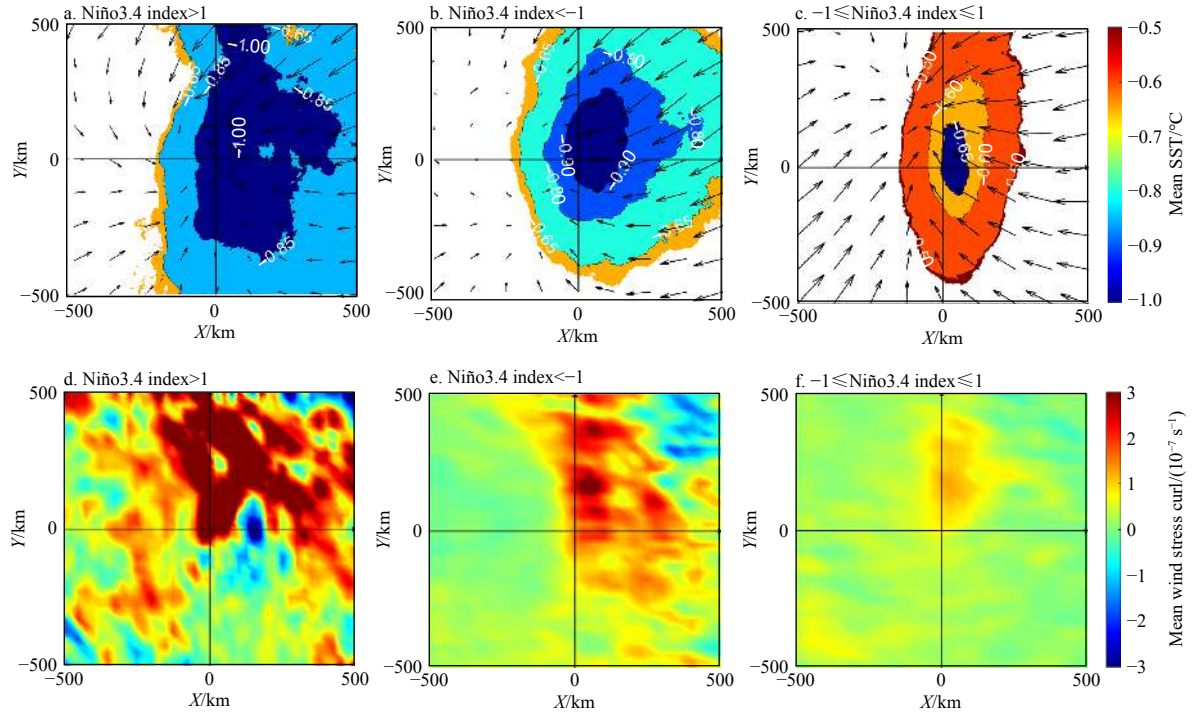

Fig. 8. Composite average wind speed (vector) and ΔSST (colour scale) (a–c), and composite wind stress curl (d–f). The composite times are separated into El Niño years, La Niña years, and normal years from left to right panels.

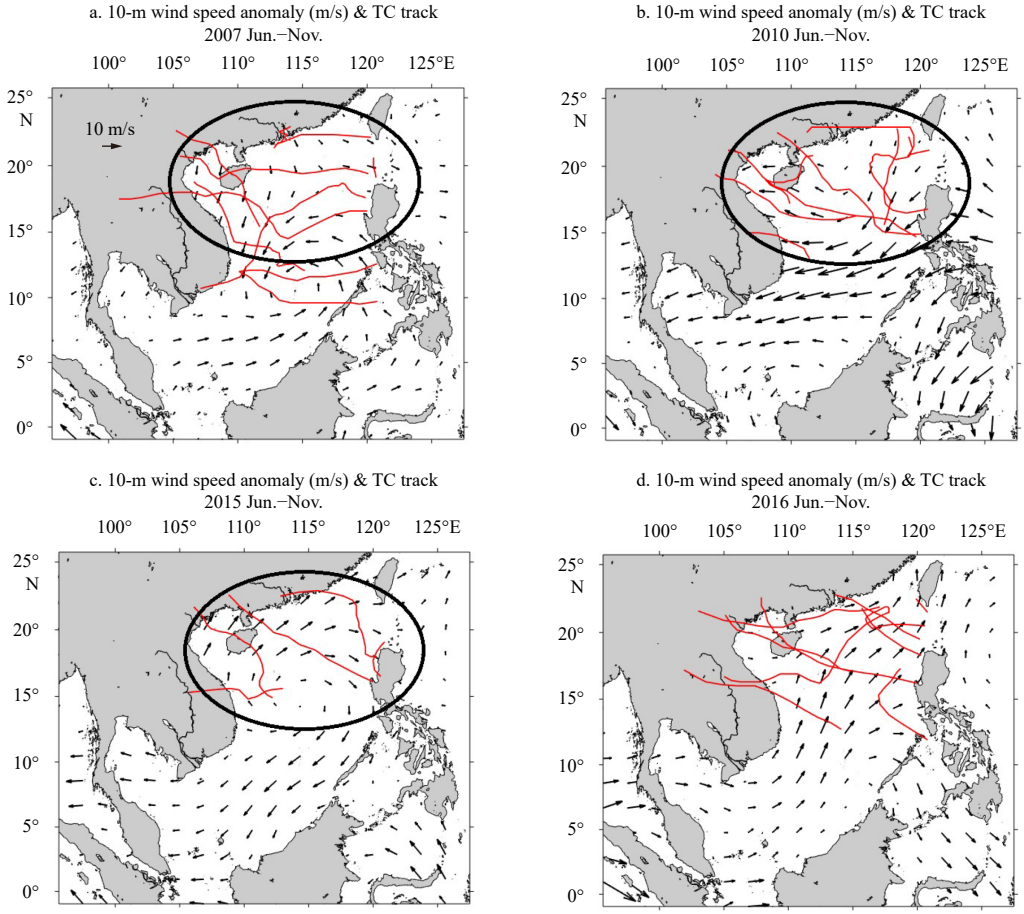

Fig. 9. 10–m wind speed anomaly in summer to autumn of 2007 (a), 2010 (b), 2015 (c), and 2016 (d). The wind anomaly was compared to mean wind speed in summer to autumn of 2006–2018. The red lines are tropical cyclone (TC) tracks. The black circles are the anticyclone position.

we need to use mixed layer heat balances model for further study.

5 Conclusions

Interannual variability in TCSSC was investigated in the SCS. The mean TCSSC zone (<–0.7°C) covered approximately 50 000 km^2. Both the magnitude and area of TCSSC exhibited significant interannual variability. The translation speed of TC was an important factor in the interannual variability in TCSSC. The absolute magnitude of TCSSC decreased gradually, except during El Niño years. El Niño events were suggested to regulate the interannual variability in TCSSC via triggering anticyclones over the SCS, which brought pre-TC high SSTs and shallow mixed layer. The types of El Niño events also influenced break-up time of the peak values of TCSSC, that is, the peak values occurred during the developing stage of EP El Niño event and the decaying stage of CP El Niño events.

A notable 6-month time-lag of El Niño and ΔSST occurred from 2006 to 2015. The anticyclone started from spring, and the TCSSC get enhanced in the following summer-autumn. This time-lag among El Niño, anticyclone and ΔSST merits future study.

Acknowledgements

TC information data are from http://tcdata.typhoon.org.cn/zjljsjj_zlhq.html and JMA (http://www.jma.go.jp/jma/jma-eng/jma-center/rsmc-hp-pub-eg/trackarchives.html). OSTIA SST data are from http://data.nodc.noaa.gov/ghrsst/L4/GLOB/UKMO/OSTIA and WindSat ocean surface wind vector were downloaded from http://data.remss.com/windsat/. Argo data were from website of https://argo.ucsd.edu/. Thanks to Lei Yang from the South China Sea Institute of Oceanology, Chinese Academy Sciences.

References

Argo. 2021. Argo float data and metadata from Global Data Assembly Centre (Argo GDAC). SEANOE, https://www.seanoe.org/data/00311/42182/, (2021-08-06)[2021-08-20], doi: 10.17882/42182

Brand S. 1971. The effects on a tropical cyclone of cooler surface waters due to upwelling and mixing produced by a prior tropical cyclone. Journal of Applied Meteorology and Climatology, 10(5): 865–874, doi: 10.1175/1520-0450(1971)010<0865:TEOATC>2.0.CO;2

Chan J C L. 2000. Tropical cyclone activity over the western North Pacific associated with El Niño and La Niña events. Journal of Climate, 13(16): 2960–2972, doi: 10.1175/1520-0442(2000)013<2960:TCAOTW>2.0.CO;2

Chang Yating, Lin I I, Huang H C, et al. 2020. The association of typhoon intensity increase with translation speed increase in the South China Sea. Sustainability, 12(3): 939, doi: 10.3390/su12030939

Chiang T L, Wu C R, Oey L Y. 2011. Typhoon Kai-Tak: An ocean's perfect storm. Journal of Physical Oceanography, 41(1): 221–233, doi: 10.1175/2010JPO4518.1

Chu P C, Veneziano J M, Fan Chenwu, et al. 2000. Response of the South China Sea to tropical cyclone Ernie 1996. Journal of Geophysical Research: Oceans, 105(C6): 13991–14009, doi: 10.1029/2000JC900035

Cione J J, Uhlhorn E W. 2003. Sea surface temperature variability in hurricanes: Implications with respect to intensity change. Monthly Weather Review, 131(8): 1783–1796, doi: 10.1175//2562.1

D'Asaro E, Black P, Centurioni L, et al. 2011. Typhoon-ocean interaction in the Western North Pacific: Part 1. Oceanography, 24(4): 24–31, doi: 10.5670/oceanog.2011.91

D'Asaro E A, Sanford T B, Niiler P P, et al. 2007. Cold wake of hurricane Frances. Geophysical Research Letters, 34(15): L15609

Dare R A, McBride J L. 2011. Sea surface temperature response to tropical cyclones. Monthly Weather Review, 139(12): 3798–3808, doi: 10.1175/MWR-D-10-05019.1

Goh A Z C, Chan J C L. 2010. Interannual and interdecadal variations of tropical cyclone activity in the South China Sea. International Journal of Climatology, 30(6): 827–843, doi: 10.1002/joc.1943

Hazelworth J B. 1968. Water temperature variations resulting from hurricanes. Journal of Geophysical Research, 73(16): 5105–5123, doi: 10.1029/JB073i016p05105

Jansen M F, Ferrari R, Mooring T A. 2010. Seasonal versus permanent thermocline warming by tropical cyclones. Geophysical Research Letters, 37(3): L03602

Ko D S, Chao S Y, Wu C C, et al. 2014. Impacts of typhoon Megi (2010) on the South China Sea. Journal of Geophysical Research: Oceans, 119(7): 4474–4489, doi: 10.1002/2013JC009785

Large W G, Pond S. 1981. Open ocean momentum flux measurements in moderate to strong winds. Journal of Physical Oceanography, 11(3): 324–336, doi: 10.1175/1520-0485(1981)011<0324:OOMFMI>2.0.CO;2

Leipper D F. 1967. Observed ocean conditions and hurricane Hilda, 1964. Journal of the Atmospheric Sciences, 24(2): 182–186, doi: 10.1175/1520-0469(1967)024<0182:OOCAHH>2.0.CO;2

Lin I I. 2012. Typhoon-induced phytoplankton blooms and primary productivity increase in the western North Pacific subtropical ocean. Journal of Geophysical Research: Oceans, 117(C3): C03039

Lin I I, Liu W T, Wu C C, et al. 2003a. New evidence for enhanced ocean primary production triggered by tropical cyclone. Geophysical Research Letters, 30(13): 1718

Lin I I, Liu W T, Wu C C, et al. 2003b. Satellite observations of modulation of surface winds by typhoon-induced upper ocean cooling. Geophysical Research Letters, 30(3): 1131, doi: 10.1029/2002GL015674

Lin I I, Wu C C, Emanuel K A, et al. 2005. The interaction of supertyphoon Maemi (2003) with a warm ocean eddy. Monthly Weather Review, 133(9): 2635–2649, doi: 10.1175/MWR3005.1

Mei Wei, Lien C C, Lin I I, et al. 2015. Tropical cyclone-induced ocean response: A comparative study of the South China Sea and tropical Northwest Pacific. Journal of Climate, 28(15): 5952–5968, doi: 10.1175/JCLI-D-14-00651.1

Mei Wei, Pasquero C. 2013. Spatial and temporal characterization of sea surface temperature response to tropical cyclones. Journal of Climate, 26(11): 3745–3765, doi: 10.1175/JCLI-D-12-00125.1

Price J F. 1981. Upper ocean response to a hurricane. Journal of Physical Oceanography, 11(2): 153–175, doi: 10.1175/1520-0485(1981)011<0153:UORTAH>2.0.CO;2

Price J F, Morzel J, Niiler P P. 2008. Warming of SST in the cool wake of a moving hurricane. Journal of Geophysical Research: Oceans, 113(C7): C07010

Price J F, Sanford T B, Forristall G Z. 1994. Forced stage response to a moving hurricane. Journal of Physical Oceanography, 24(2): 233–260, doi: 10.1175/1520-0485(1994)024<0233:FSRTAM>2.0.CO;2

Schade L R, Emanuel K A. 1999. The ocean's effect on the intensity of tropical cyclones: Results from a simple coupled atmosphere-ocean model. Journal of the Atmospheric Sciences, 56(4): 642–651, doi: 10.1175/1520-0469(1999)056<0642:TOSEOT>2.0.CO;2

Shay L K, Black P G, Mariano A J, et al. 1992. Upper ocean response to Hurricane Gilbert. Journal of Geophysical Research: Oceans, 97(C12): 20227–20248, doi: 10.1029/92JC01586

Sriver R L, Huber M. 2010. Modeled sensitivity of upper thermocline properties to tropical cyclone winds and possible feedbacks on the Hadley circulation. Geophysical Research Letters, 37(8): L08704

Stark J D, Donlon C J, Martin M J, et al. 2007. OSTIA: An operational, high resolution, real time, global sea surface temperature analysis system. In: OCEANS 2007-Europe. Aberdeen, UK: IEEE, 1–4

Wang Guihua, Su Jilan, Ding Yihui, et al. 2007. Tropical cyclone gen-

esis over the South China Sea. Journal of Marine Systems, 68(3–4): 318–326

Wang Xin, Tan Wei, Wang Chunzai. 2018. A new index for identifying different types of El Niño Modoki events. Climate Dynamics, 50(7–8): 2753–2765

Wang Guihua, Wu Lingwei, Johnson N C, et al. 2016. Observed three-dimensional structure of ocean cooling induced by Pacific tropical cyclones. Geophysical Research Letters, 43(14): 7632–7638, doi: 10.1002/2016GL069605

Wang Bin, Yang Jing, Zhou Tianjun, et al. 2008. Interdecadal changes in the major modes of Asian-Australian monsoon variability: Strengthening relationship with ENSO since the Late 1970s. Journal of Climate, 21(8): 1771–1789, doi: 10.1175/2007JCLI1981.1

Wu Renguang, Chen Wen, Wang Guihua, et al. 2014. Relative contribution of ENSO and East Asian winter monsoon to the South China Sea SST anomalies during ENSO decaying years. Journal of Geophysical Research: Atmospheres, 119(9): 5046–5064, doi: 10.1002/2013JD021095

Ying Ming, Zhang Wei, Yu Hui, et al. 2014. An overview of the China meteorological administration tropical cyclone database. Journal of Atmospheric and Oceanic Technology, 31(2): 287–301, doi: 10.1175/JTECH-D-12-00119.1

Yuan Yuan, Yang Song, Zhang Zuqiang. 2012. Different evolutions of the Philippine Sea Anticyclone between the Eastern and Central Pacific El Niño: Possible effects of Indian Ocean SST. Journal of Climate, 25(22): 7867–7883, doi: 10.1175/JCLI-D-12-00004.1

Zhao Haikun, Wang Chunzai. 2019. On the relationship between ENSO and tropical cyclones in the western North Pacific during the boreal summer. Climate Dynamics, 52(1–2): 275–288